

Satellite-observed pantropical carbon dynamics

Lei Fan, Jean-Pierre Wigneron, Philippe Ciais, Jérôme Chave, Martin Brandt, Rasmus Fensholt, Sassan Saatchi, Ana Bastos, Amen Al-Yaari, Koen Hufkens, et al.

▶ **To cite this version:**

Lei Fan, Jean-Pierre Wigneron, Philippe Ciais, Jérôme Chave, Martin Brandt, et al.. Satellite-observed pantropical carbon dynamics. Nature Plants, 2019, 5 (9), pp.944-951. 10.1038/s41477-019-0478-9 . hal-02403129

HAL Id: hal-02403129
https://hal.science/hal-02403129v1

Submitted on 8 Oct 2025

HAL is a multi-disciplinary open access archive for the deposit and dissemination of scientific research documents, whether they are published or not. The documents may come from teaching and research institutions in France or abroad, or from public or private research centers.

L'archive ouverte pluridisciplinaire **HAL**, est destinée au dépôt et à la diffusion de documents scientifiques de niveau recherche, publiés ou non, émanant des établissements d'enseignement et de recherche français ou étrangers, des laboratoires publics ou privés.



Distributed under a Creative Commons CC BY 4.0 - Attribution - International License

LETTERS
https://doi.org/10.1038/s41477-019-0478-9

nature plants

Satellite-observed pantropical carbon dynamics

Lei Fan[1,2], Jean-Pierre Wigneron[2*], Philippe Ciais[3*], Jérôme Chave[4], Martin Brandt[5], Rasmus Fensholt[5], Sassan S. Saatchi[6,7], Ana Bastos[8], Amen Al-Yaari[2], Koen Hufkens[2,9], Yuanwei Qin[10], Xiangming Xiao[10], Chi Chen[11], Ranga B. Myneni[11], Roberto Fernandez-Moran[12], Arnaud Mialon[13], N. J. Rodriguez-Fernandez[13], Yann Kerr[13], Feng Tian[14] and Josep Peñuelas[15,16]

Changes in terrestrial tropical carbon stocks have an important role in the global carbon budget. However, current observational tools do not allow accurate and large-scale monitoring of the spatial distribution and dynamics of carbon stocks[1]. Here, we used low-frequency L-band passive microwave observations to compute a direct and spatially explicit quantification of annual aboveground carbon (AGC) fluxes and show that the tropical net AGC budget was approximately in balance during 2010 to 2017, the net budget being composed of gross losses of −2.86 PgC yr^{-1} offset by gross gains of −2.97 PgC yr^{-1} between continents. Large interannual and spatial fluctuations of tropical AGC were quantified during the wet 2011 La Niña year and throughout the extreme dry and warm 2015–2016 El Niño episode. These interannual fluctuations, controlled predominantly by semiarid biomes, were shown to be closely related to independent global atmospheric CO_2 growth-rate anomalies (Pearson's $r = 0.86$), highlighting the pivotal role of tropical AGC in the global carbon budget.

Tropical terrestrial biomes contribute to the interannual variability of the global terrestrial carbon balance, which in turn is essential to changes in the global atmospheric CO_2 concentration[1]. Thus, accurate monitoring of temporal and spatial changes in carbon stocks across the tropics is key for better predicting the evolution of atmospheric CO_2 over the coming century. However, at present no method exists for spatially explicit quantification of the tropical land sinks and sources[1]. Current observational tools are impeded by signal saturation in dense forests[2] and sparse spatial or temporal sampling[3], thus the spatial distribution and trends of carbon sources and sinks across the tropics remain poorly resolved[1].

Results from top-down atmospheric inversions that are consistent with vertical CO_2 profiles[4] indicate that the long-term tropical net CO_2 flux is close to zero, but there are too few in situ surface CO_2 stations to distinguish carbon sinks from tropical forest regrowth and carbon sources from deforestation. Bottom-up approaches using ground forest inventory and satellite data suggest that tropical deforestation represents large emissions 0.57–1.3 PgC yr^{-1} (refs. [5–7]). A more diffuse carbon sink is observed in undisturbed and regrowing forests[8], but a decline of the forest carbon sink in the Amazon[9] and a strong reduction of this sink during extreme EI Niño events have also been reported[10]. However, forest inventory data are also scarce in the tropics[1] and semiarid woody biomes are critically under-sampled, even though they cover 40% of the tropical land area[11].

The interannual variability of carbon fluxes from tropical land to the atmosphere is also coupled with climatic conditions, and the increased frequency of drought events is a threat to tropical forest biomes[12]. Major droughts in 2005, 2010 and 2015–2016 represent a testing ground for understanding how the frequency of extreme climatic events may affect the carbon balance in future. Recent studies suggest that the tropics switched to acting as a net source during the 2015–2016 EI Niño[13–15], findings that are supported by model simulations[16]. However, observations of the spatial distribution of this major flux anomaly are still unavailable, limiting the attribution of the EI Niño anomaly to specific tropical continents and biomes[1].

Remote sensing is poised to advance the mapping of vegetation structure and quantify the stocks and changes of aboveground carbon (AGC) in vegetation[3,5,17]. Although static maps of AGC have been produced from remote sensing[3,5,18,19], these maps generally differ in terms of both magnitude and spatial patterns and are available for only a single epoch, and therefore cannot be used to assess interannual variations in carbon stocks[17].

Vegetation optical depth (VOD), retrieved from passive microwave satellite observations and related to the water content of vegetation mass[20–22], offers possibilities for monitoring AGC dynamics[15,23,24] because of its key features: frequent observations that provide daily tropical coverage and independence of the effects of atmospheric and cloud contamination[23]. The new VOD product used in this study, hereafter L-VOD, has recently been produced using low-frequency (L-band, 1.4 GHz) microwave observations from the Soil Moisture and Ocean Salinity (SMOS) satellite[25,26]. The radiometer onboard the SMOS satellite has superior sensitivity to carbon density than previous higher-frequency passive microwave VOD products and is able to retrieve the overall AGC stocks even in dense tropical ecosystems[15,27,28]. By contrast, high-frequency VOD products[29] saturate in vegetation with carbon stocks higher than 100 MgC ha^{-1} (ref. [23]).

Here, we used L-VOD to derive spatially explicit representations of changes in AGC (Methods) during 2010–2017 across the pantropics (consisting of tropical America, Africa and Asia between 23.45° N and 23.45° S, excluding Australia), which are known to have a

[1]School of Geographical Sciences, Nanjing University of Information Science and Technology, Nanjing, China. [2]ISPA, UMR 1391, INRA Nouvelle-Aquitaine, Villenave d'Ornon, France. [3]Laboratoire des Sciences du Climat et de l'Environnement, CEA/CNRS/UVSQ/Université Paris Saclay, Gif-sur-Yvette, France. [4]Laboratoire Evolution et Diversité Biologique, Université Paul Sabatier, Toulouse, France. [5]Department of Geosciences and Natural Resource Management, University of Copenhagen, Copenhagen, Denmark. [6]Jet Propulsion Laboratory, California Institute of Technology, Pasadena, CA, USA. [7]Institute of the Environment and Sustainability, University of California, Los Angeles, CA, USA. [8]Department of Geography, Ludwig-Maximilians Universität, Munich, Germany. [9]Department of Applied Ecology and Environmental Biology, Ghent University, Ghent, Belgium. [10]Department of Microbiology and Plant Biology, Center for Spatial Analysis, University of Oklahoma, Norman, OK, USA. [11]Department of Earth and Environment, Boston University, Boston, MA, USA. [12]Image Processing Laboratory, University of Valencia, Valencia, Spain. [13]CESBIO, Université de Toulouse, CNES/CNRS/INRA/IRD/UPS, Toulouse, France. [14]Department of Physical Geography and Ecosystem Science, Lund University, Lund, Sweden. [15]CSIC, Global Ecology Unit CREAF-CSIC-UAB, Bellaterra, Spain. [16]CREAF, Cerdanyola del Vallès, Spain. *e-mail: jean-pierre.wigneron@inra.fr; philippe.ciais@lsce.ipsl.fr

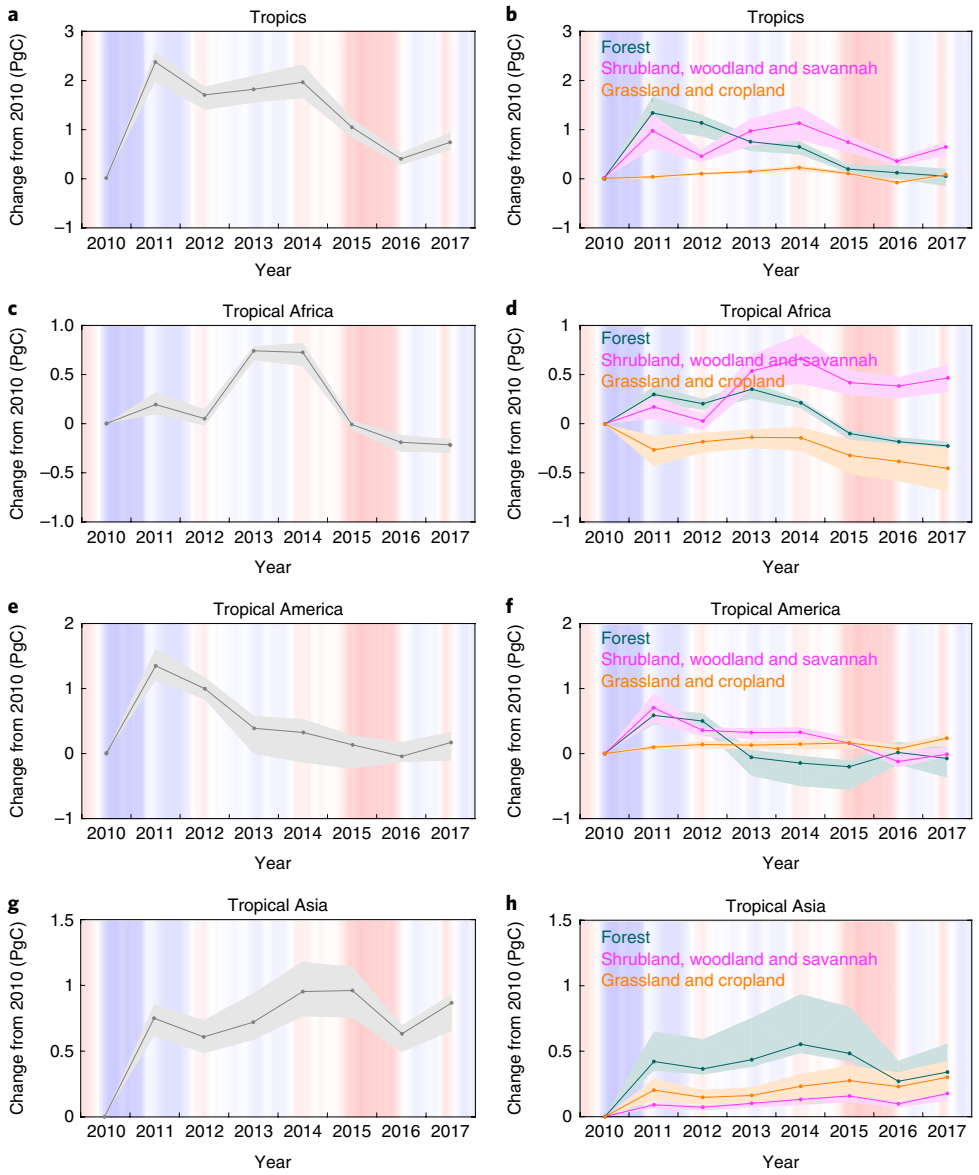


Fig. 1 | Temporal variations in annual AGC in the tropics (continents and biomes), expressed as the difference from 2010 values. a,**c**,**e**,**g**, Annual variations in AGC in the tropics (**a**; $n = 51{,}395$) and in the tropical regions of Africa (**c**; $n = 25{,}058$), America (**e**; $n = 19{,}777$) and Asia (**g**; $n = 6{,}560$), respectively. **b**,**d**,**f**,**h**, Corresponding changes in AGC are shown for three biomes (forest; shrubland, woodland and savannah; grassland and cropland) in the tropics (**b**) and in the tropical regions of Africa (**d**), America (**f**) and Asia (**h**), respectively. The ranges represented by shading around the line show the minimum and maximum of AGC changes estimated by ten calibrations (Supplementary Table 1). The background shading shows the intensity of La Niña (blue) and El Niño (red) events defined by MEI.

pivotal role in the global terrestrial carbon sink[1]. The L-VOD dataset enabled us to gain insights into the dynamics of tropical AGC and the covariation with climate, anthropogenic forest cover disturbances and changes in the global atmospheric CO_2 concentration.

During 2010–2017, tropical AGC change represented a small net increase of +0.11 [+0.08,+0.13] PgC yr^{-1} (the range represents the minimum and maximum of AGC changes estimated by ten calibrations; a positive value indicates net accumulation (sink) of carbon in aboveground biomes; Fig. 1a). This net carbon budget is composed of gross losses of −2.86 [−2.31, −3.05] PgC yr^{-1} offset by gross gains of +2.97 [+2.41, +3.15] PgC yr^{-1} estimated at the spatial resolution of the SMOS grid (25 × 25 km). Tropical Asia was a net mean sink of +0.12 [+0.09, +0.13] PgC yr^{-1} (Fig. 1g) and tropical Africa and South America were almost neutral with a flux of −0.03 [−0.04, −0.02] PgC yr^{-1} (Fig. 1c) and +0.02 [−0.02, +0.05] PgC yr^{-1} (Fig. 1e), respectively. Carbon stocks increased slightly in woodland, shrubland and savannah regions, particularly in tropical Africa, whereas changes in forest, grassland and cropland were close to zero (Fig. 1b).

Over the study period, AGC peaked in 2011 in response to the strong La Niña event and decreased subsequently over the tropics (Fig. 1a). Strong La Niña conditions prevailed from late 2010 to early 2012[30] (Fig. 1a), resulting in a transient increase of tropical AGC of +2.36 [+1.97,+2.57] PgC, mainly from tropical America (+1.34 [+1.13,+1.61] PgC; Fig. 1e) and Asia (+0.75 [+0.61,+0.84] PgC; Fig. 1g). In tropical America, the peak of AGC in 2011 is mainly observed in forests and shrublands or savannahs and suggests recovery of vegetation following the 2010 drought (Fig. 1a), mainly driven by a wet climatic anomaly (Supplementary Fig. 13a and Supplementary Text 6).

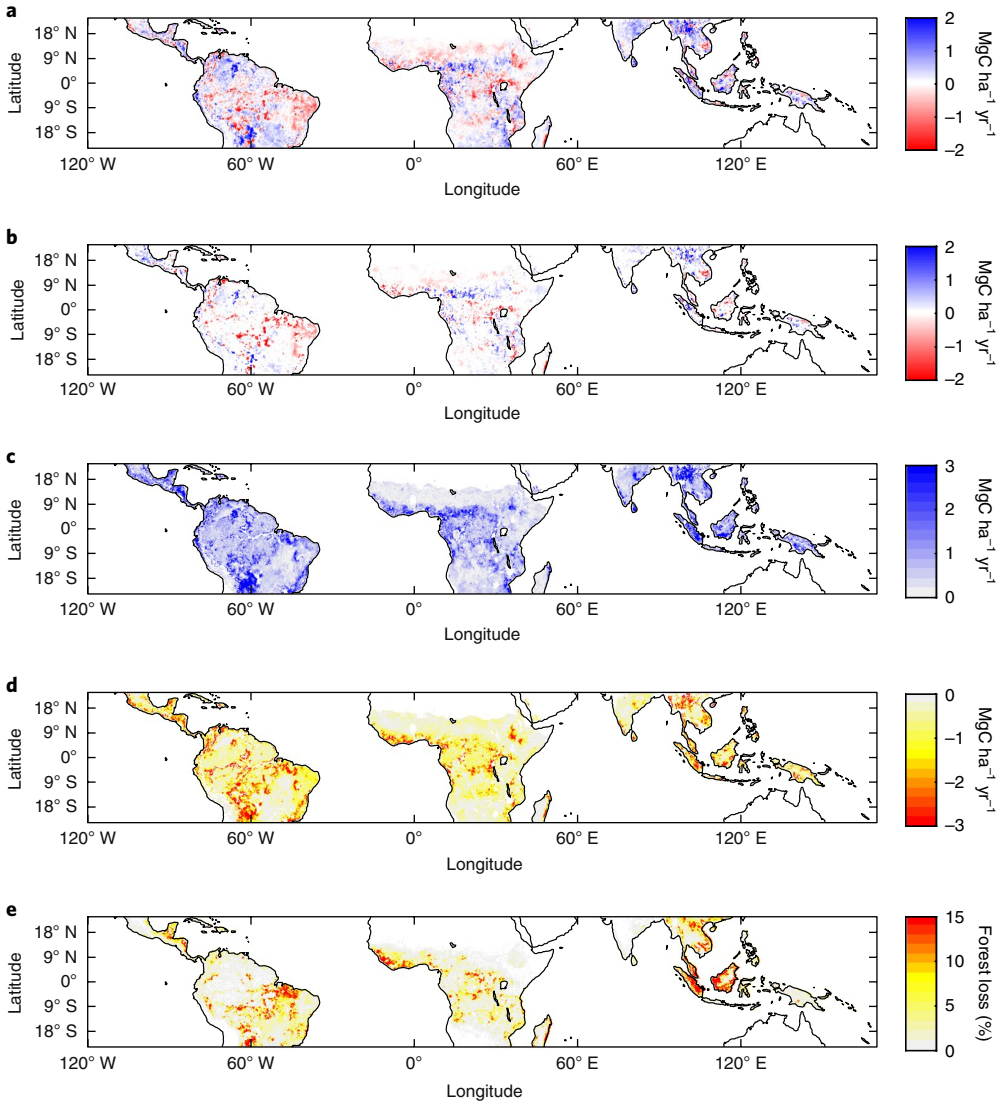


Fig. 2 | Spatial patterns and trends in tropical carbon changes. a–e, Yearly net changes (**a**), trends (**b**), gross gains (**c**) and gross losses (**d**) in AGC, and yearly net changes in forest-loss rates[31] (**e**) for 2010–2017. Yearly net changes, trends and gross gains and losses in AGC were estimated on the basis of the medians of the changes in AGC estimated by ten sets of the fitted relationships between L-VOD and AGC ($n = 51{,}395$, 11,992, 51,361 and 47,199 for **a–d**, respectively). Yearly trends in AGC are represented by significantly positive and negative trends (linear trend; $P < 0.05$). Gross losses in AGC are calculated by cumulating negative changes in AGC for consecutive years from 2010 to 2017.

A strong El Niño event developed in mid-2015 and persisted until mid-2016 (Fig. 1a)[13]. This event caused a drop of tropical AGC of −0.95 [−1.00, −0.76] PgC in 2015—of which −0.74 [−0.86, −0.62] PgC was in Africa (Fig. 1c) and −0.20 [−0.26, −0.1] PgC was in America (Fig. 1e)—which was attributed mainly to extremely dry and warm climatic conditions (Supplementary Fig. 13a and Supplementary Text 6). The 2015 loss in Africa occurred in all biomes, with the largest losses in woodland, shrubland and savannah regions. By contrast, carbon losses and gains were evenly balanced in tropical Asia in 2015. Of note, AGC losses continued in 2016, with a biomass loss of −0.65 [−0.82, −0.38] PgC, mostly in Asia (−0.35 [−0.50, −0.26] PgC) followed by Africa (−0.19 [−0.22, −0.15] PgC) and America (−0.12 [−0.3, +0.11] PgC), in response to more severe anomalies in both surface soil moisture and land surface temperature in 2016 compared with 2015 (Supplementary Fig. 13a and Supplementary Text 6). Combining the two years 2015 and 2016 together, the average AGC carbon losses (−0.80 [−0.59, −0.96] PgC yr^{-1}) are in the range of the net land–atmosphere abnormal CO_2 source simulated by land surface models (−1.1 [−2.5, +0.1] PgC yr^{-1})[16].

Pixels with more than 5% forest losses (covering 16% of the tropics) as identified by Hansen et al.[31] (Methods), displayed a net carbon loss of −0.09 [−0.14, −0.07] PgC yr^{-1} in the aboveground vegetation compartment for 2010–2017 (Supplementary Table 2). Net carbon losses due to deforestation were offset by a net carbon uptake of +0.20 [+0.14, +0.24] PgC yr^{-1} across pixels with less than 5% deforestation. This sink was found mainly in tropical Asia (+0.10 [+0.06, +0.13] PgC yr^{-1}) and America (+0.09 [+0.06, +0.12] PgC yr^{-1}). Trends for 2010–2017 showed carbon losses in the arc of deforestation of southern Amazonia, in the Democratic Republic of Congo and in Indonesia (Fig. 2a,b). The carbon uptake was found in the Central African Republic and in the northernmost regions of tropical Asia and Central America (Fig. 2a,b).

We defined gross carbon losses as accumulated yearly losses, excluding regrowth years. Overall, gross carbon loss from areas of deforestation (forest losses >5%) was −0.78 [−0.61, −1.04] PgC yr^{-1}

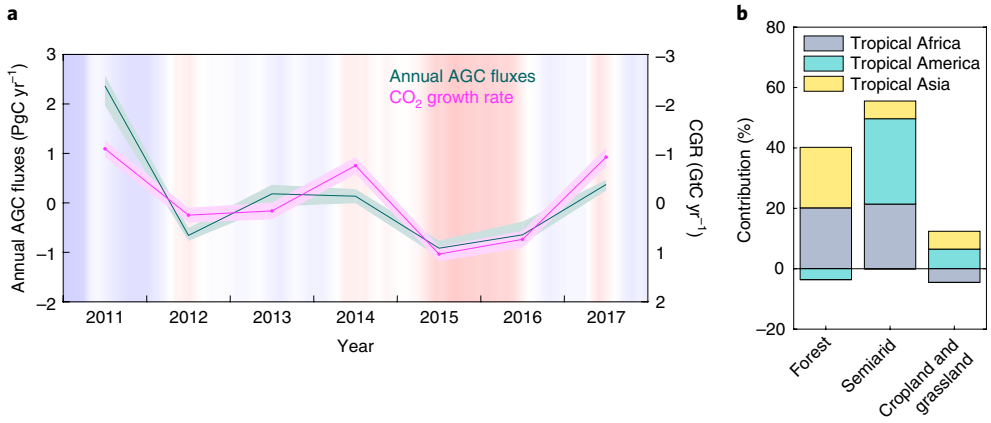


Fig. 3 | Interannual variability of global atmospheric CGR and tropical AGC fluxes. a, The interannual variability in the atmospheric CGR (right axis) and AGC (left axis) fluxes was calculated by removing trends from annual atmospheric CGR and AGC fluxes, respectively, over 2011–2017. The tropical annual AGC fluxes were calculated using net AGC changes for individual years (compared to the previous year; $n=7$). The vertical axis is inverted for the de-trended CGR so that positive (downwards) anomalies indicate a weaker land carbon sink. The ranges represented by shading around the lines of AGC and CGR show the minimum and maximum of AGC changes estimated by ten calibrations and the uncertainties in CGR, respectively. **b**, Contribution (%) of land-cover classes and continent to the interannual variability in tropical AGC fluxes. Tropical semiarid biomes consist of shrubland, woodland and savannah[39]. The contributions (%) of the different biomes and regions to the tropical AGC fluxes were estimated using the method described in Ahlström et al.[39].

(Supplementary Table 2 and Supplementary Fig. 1b). Areas with high gross carbon loss (Fig. 2d) matched well with areas where tropical forest cover decreased (Fig. 2e) in the dataset of Hansen et al.[31] (Methods) (as an illustration, results obtained over a deforestation and an afforestation site are shown in Supplementary Fig. 2). Carbon gains in Central America, southern and northern regions of tropical America, Central African Republic and in the northernmost regions of tropical Asia and India reflect high recovery rates (Fig. 2c) offsetting carbon losses (Fig. 2d) leading to an overall net carbon storage in these regions (Fig. 2a). The spatial patterns of the areas showing carbon sinks agree well with greening regions as evaluated by Chen et al.[32] (Supplementary Fig. 3). In parallel, a spatial agreement between regions showing browning trends and carbon losses was found in eastern tropical Africa and the tropical rainforests of Madagascar.

There is an ongoing debate about the role of humid versus semiarid tropical biomes in controlling the global atmospheric CO_2 growth rate (CGR)[33,34]. We found a strong association between yearly de-trended global atmospheric CGR measured from the National Oceanic and Atmospheric Administration Earth System Research Laboratory[35] and annual tropical AGC fluxes as inferred above ($r=0.86$, $P=0.03$, $n=7$; Fig. 3a), supporting previous findings[36–38] that tropical biomes dominate the interannual variability in atmospheric CGR. Carbon losses of biomass (−1.6 [−1.82, −1.14] PgC) during the severe 2015–2016 El Niño accounted for 90% of the anomaly in atmospheric CGR (1.7 PgC).

We evaluated the contribution of different biomes to the interannual variability of AGC by separating tropical forests[39], semiarid biomes (shrubland, woodland and savannah), cropland and grasslands. The contribution of semiarid biomes accounts for the largest fraction of the interannual variability of tropical AGC fluxes (55.5%), with a smaller contribution of forests (36.6%), and croplands and grasslands (7.9%) (Fig. 3b), suggesting that semiarid ecosystems are among the most important components of the interannual variability in the tropical AGC[30]. Interannual variability in the tropical AGC fluxes is determined predominantly by semiarid biomes from tropical America and Africa and by forests from tropical Africa and Asia. Likewise, the positive covariation (+0.19 PgC yr^{-1} (ref. [2]); Supplementary Table 3) of AGC fluxes from tropical forests and semiarid biomes suggests that both biomes act in phase to control interannual variability in AGC.

The L-VOD satellite dataset provides insights into recent spatial changes of the carbon cycle in the tropics in relation to deforestation and tropical extreme climatic events. The dataset was used to quantify both AGC losses in the tropics during the 2010 and 2015–2016 El Niño events and the subsequent recoveries in 2011 and 2017. In sum, the results show a neutral contribution of the tropics to the global carbon budget between 2010 and 2017. L-VOD revealed that the recovery in 2017 was weaker than in 2011, which could be partly attributed to the warm climatic conditions in 2017 (Supplementary Fig. 13), which negatively impacted the terrestrial carbon uptake[38,40]. Using 2011 as a reference for comparison[13], our estimations of AGC losses caused by the 2015–2016 El Niño were generally lower than estimates from the Orbiting Carbon Observatory (OCO-2)[13] (which include soil carbon, aboveground biomass and river CO_2 fluxes) over tropical America (−1.41 versus −1.60 PgC for OCO-2), Africa (−0.40 versus −0.70 PgC for OCO-2) and Asia (−0.13 versus −1.00 PgC for OCO-2). This difference could be partly attributed to the fact that our estimations of AGC do not account for ecosystem respiration rate[16] and peat fires[41], which, especially in tropical Asia, are associated with large carbon losses from soils[42,43].

Furthermore, we were able to quantify AGC losses from areas of deforestation, which were fully compensated by carbon uptakes by undisturbed forests over the entire tropics. The L-VOD based estimation of emissions from deforestation (0.78 PgC yr^{-1}) matches closely with previous estimations (for example, 0.81 PgC yr^{-1} obtained by Harris et al.[6] between 2000 and 2005), suggesting that the flux from gross tropical deforestation have remained within 0.6–0.8 PgC yr^{-1} since the early 2000s[44,45]. Moreover, we estimated AGC losses from processes other than deforestation to be 2.08 PgC yr^{-1}, caused by natural disturbances, climate-induced mortality and forest degradation, including selective removals from within forested stands (not currently included in deforestation estimates based on optical satellite data[44]). This suggests that processes other than deforestation are responsible for about twice the amount of carbon release from deforestation; however, there are large regional variations[17,46]. In addition, some of the losses in carbon may be caused by the reduction of AGC following the extreme La Niña (return to normal conditions)[47] and subsequent El Niño.

We further showed that non-deforested regions act as a carbon sink, which is supported by measurements from forest inventory

plots[48–50]. The increasing AGC trend over intact, non-disturbed forests may be attributed to a CO_2 fertilization effect on tree growth, consistent with no strong signal from widespread disturbance recovery[51] in forest plots and with model-based attribution of the recent greening trend over the tropics[52]. The carbon sink of the Sahel and South Africa are primarily driven by increasing precipitation[52,53], whereas human land-use management may be a dominant driver of carbon sink in India and northern tropical Asia[32]. Here, L-VOD data resolve the spatial distribution of this uptake over the whole tropics, showing that the net sink density in non-deforested regions was rather low between 2010 and 2017 (+0.05 MgC ha^{-1} yr^{-1}). This low carbon accumulation rate could be partly explained by a long-term increase in mortality rates[10] and the recent El Niño events[54]. This result is in contrast to the high carbon accumulation ([+1.33, +3.05] MgC ha^{-1} yr^{-1}) that was estimated from individual field plots across Amazonian secondary and managed forests[48,55]. The disagreement could also stem from the fact that the coarse spatial resolution of L-VOD (25 × 25 km) merges all aboveground biomes including disturbed forests and non-forest ecosystems, which have lower rates of gain than secondary and managed forests[17]. While carbon changes in both deforested and non-deforested areas are expected, our estimates are admittedly conservative as a result of the coarse spatial resolution of the L-VOD data, which averages gross carbon sources and sinks at scales smaller than 25 km. Gross gain and loss could thus be larger at higher spatial resolution.

AGC fluxes estimated from L-VOD, which are independent from process-based models, are consistent with the phase and amplitude of global CO_2 growth-rate anomalies. This suggests that litter and soil carbon fluxes have a smaller variability than AGC fluxes, and highlights that changes in the tropical AGC balance dominate changes in the global carbon balance. The observed spatial patterns of the contribution of terrestrial ecosystems to the total tropical interannual variability in AGC fluxes (Supplementary Fig. 4) agreed with model results[39]. This supports the model-based findings that semiarid biomes can have profound impacts on the interannual variability of the global carbon cycle[30]. From observational data we revealed spatial patterns over recent years showing: (1) the main positive contributions are found in the eastern and northern regions of the Amazon basin, southeastern regions of Africa, and Asia; (2) the main regions with negative contributions are found in forested regions in tropical America (for instance, in the arc of deforestation in the Amazon basin), and non-forested regions (for example, semiarid biomes and croplands and grasslands) in tropical Africa. These negative contributions could be mainly attributed to both human activities (for example, deforestation and high population growth)[56] and the different sensitivities of biomes to climate variations among regions[39].

The L-VOD data provide direct and spatially explicit remote-sensing information that scales up to annual tropical AGC anomalies. This product overcomes several of the limitations of current tools used to estimate the tropical land sink. The coarse resolution (25 × 25 km) of L-VOD limits its applicability for detailed regional analysis, but is not a limitation for addressing the critical role of the terrestrial land sink on changing atmospheric characteristics. On the basis of L-VOD, a direct observational estimate of the pan-tropical carbon sink could be clearly related, in terms of correlation and magnitude, to the observed CGR in recent years. The results show the applicability of L-VOD for monitoring, in near-real time, spatiotemporal changes in AGC to reveal hotspot areas of changes due to human activity (deforestation) and climate variability (such as El Niño/Southern Oscillation) at large scale. The data and results shown here hold promise for data-informed process-based Earth-system models to better predict the future of land carbon sinks, and to further reconcile divergent estimates of carbon sources and sinks derived from modelling approaches (bottom-up[5–7] as well as top-down[54]) and observational systems[17].

Methods

The L-VOD index used in this study is sensitive to the total vegetation water content (VWC, Mg ha^{-1})[28]. The relationship between L-VOD and VWC is nearly linear[25,57]. L-VOD for woody vegetation is mainly sensitive to the water content of stems and branches, so the effects of leaves can be neglected in the first order[28]. Moreover, a specificity of SMOS is its multiangular capability, which enables a robust decoupling of the effects of soil moisture and vegetation opacity (parameterized by L-VOD)[28]. This capability arises from the design of the synthetic-aperture imaging antenna of the SMOS L-band microwave radiometer and is exploited in the SMOS-IC algorithm, which is based on the original SMOS algorithm[58] as defined for the European Space Agency Earth Explorer mission call. The principle of the algorithm is to retrieve simultaneously both soil moisture and L-VOD for 'rich' SMOS observational configurations (for example, when a large range of multiangular observations is available) and to benefit from the slow time variations of L-VOD for 'poor' SMOS observational configurations (for example, when a narrow range of multiangular observations is available). The high accuracy of both the SMOS-IC soil moisture and L-VOD products have been evaluated in several recent studies[15,16,27,28,59].

We assumed that the yearly average of the per cent moisture content of stems and branches for woody vegetation at the spatial scale of the SMOS grid (25 × 25 km) was relatively constant between years, so that the yearly average of vegetation water content and dry biomass would be strongly correlated over time. This assumption is supported by several studies reporting the strong relationship between L-VOD and biomass for woody vegetation being almost linear and independent of the year of calculation[15,27]. The yearly average of L-VOD, on the basis of its strong link to vegetation water content, can thus be considered as a robust proxy of biomass. Other remotely sensed estimates or proxies of biomass have been used to estimate the annual changes in AGC at continental scales, such as LiDAR estimates of canopy height[3,5], high-frequency VOD[23] or radar backscattering[3]. Radar backscattering was strongly sensitive to forest structure, but its relationship to biomass is highly nonlinear at L-band[19]. The computation of L-VOD in the SMOS-IC version is independent of the use of these indexes, making it a new and complementary tool for monitoring AGC.

L-VOD is more closely related to AGC density (coefficient of determination, $r^2 = 0.81–0.86$) compared with high-frequency VOD products at C-, X- and K-band[23] (C/X/K-VOD; $r^2 = 0.53–0.63$) and enhanced vegetation index (EVI) ($r^2 = 0.42–0.65$) over the tropics (Supplementary Fig. 5), which is in line with previous findings over Africa[15,27]. The relationship between AGC and C/X/K-VOD (Supplementary Fig. 5b, e, h and k) has a similar shape to that of AGC versus L-VOD (Supplementary Fig. 5a, d, g and j) but C/X/K-VOD shows a stronger saturation at high AGC values relatively to L-VOD. EVI shows some sensitivity to AGC for low AGC values (with a low slope) but clear saturation effects are found for medium or high AGC values (Supplementary Fig. 5c,f,i,l).

AGC was first retrieved from the L-VOD product on the basis of an empirical calibration of the spatial relationships linking L-VOD to reference AGC gridded datasets, as in Brandt et al.[15]. The reference AGC datasets were obtained from static benchmark maps (corresponding to average values over a few years). Assuming that a good calibration can be achieved, the SMOS L-VOD product adds a temporal dimension to static maps provided that a 'space for time' substitution holds true[15]. Annual changes in AGC are quantified as explained below and compared with several vegetation and climatic variables to analyse the response of AGC to deforestation and recent climatic events.

As an illustration of the ability of L-VOD to capture deforestation, degradation and forest regrowth events, comparisons have been made using forest dynamics information resolved with higher spatial resolution (Landsat and Moderate Resolution Imaging Spectroradiometer (MODIS)-based information). Large forest area losses caused by mining can be observed between December 2009 and December 2016 in Landsat imagery (Supplementary Fig. 2a,b) as well as from the MOD100 forest area dataset (Supplementary Fig. 2c). The estimates of the AGC changes retrieved from L-VOD (Supplementary Fig. 2c) are strongly correlated with MODIS-derived forest area ($r = 0.94$, $P < 0.01$, $n = 8$). Similarly, the high sensitivity of AGC to changes in forest area was also found in a region with afforestation and forest regrowth (Supplementary Fig. 2d–f, $r = 0.94$, $P < 0.01$, $n = 8$).

Benchmark maps of AGC density. Brandt et al.[15] used the maps produced by Baccini et al.[5] to calibrate the L-VOD–AGC relationship for Africa. Here we used four static AGC benchmark maps (Supplementary Fig. 7a–d and Supplementary Text 2) to calibrate L-VOD and retrieve AGC to reduce the dependence of our results on the accuracy of a single biomass map. These maps include three pantropical maps published by Saatchi et al.[3], Avitabile et al.[18] and Baccini et al.[5], hereafter referred to as the 'Saatchi', 'Avitabile' and 'Baccini' maps, respectively. The Saatchi map used in the present study is an updated version that represents AGC circa 2015[3,60]. A fourth map covering only Africa was produced by extending the dataset by Bouvet et al.[19] to higher AGC values using the dataset by Mermoz et al.[61], described by Rodriguez-Fernandez et al.[27], hereafter referred to as the 'Bouvet–Mermoz' map. The original units of aboveground biomass density (Mg ha^{-1}) were converted to AGC density (MgC ha^{-1}) by multiplying the original values by a factor of 0.5 (ref. [5]). All AGC maps were aggregated to 25 km spatial resolution to match

the spatial resolution of the SMOS data by averaging AGC pixels within the SMOS-grid cells.

SMOS-IC soil moisture, L-VOD and the retrieved AGC products. Changes in AGC were estimated from the L-VOD product using SMOS datasets in the SMOS-IC version. The SMOS-IC product[26] provides data for global daily L-VOD and soil moisture data from the descending and ascending orbits covering the period from 12 January 2010 to 31 December 2017 at a spatial resolution of 25 km (Supplementary Table 4 and Supplementary Fig. 7f). The SMOS-IC L-VOD and soil moisture data were retrieved simultaneously from a two-parameter inversion of the L-band microwave emission of the biosphere (L-MEB) model from the multiangular and dual-polarized SMOS observations[62]. In the newly developed SMOS-IC algorithm, L-VOD and soil moisture are retrieved without external vegetation or hydrologic products as inputs in the L-MEB inversion model. L-VOD retrievals thus depend only on temperature fields from the European Centre for Medium-Range Weather Forecasts for calculating the effective surface temperature, and are independent of any vegetation index, unlike previous VOD products from SMOS[63].

The root mean square (r.m.s.) error between the measured and simulated brightness temperature (referred to as r.m.s. error-TB) associated with the SMOS-IC product was used to filter out observations affected by radio frequency interference (RFI), which perturbs the natural microwave emission from the Earth surface measured by passive microwave systems[64,65]. We excluded daily observations, influenced by RFI effects, for which r.m.s. error-TB was larger than 8 K (ref. [15]). Robust estimates of annual L-VOD and soil moisture were then obtained as the medians of all high-quality ascending and descending retrievals with more than 30 valid observations per year (Supplementary Text 3). This filtering left a large fraction of the original SMOS pixels available for the analysis in tropical America (85.2%), Africa (86.6%) and Asia (68.5%). Relative to tropical America and Africa, many regions in tropical Asia were more affected by RFI effects, especially for ascending orbits.

The yearly L-VOD data were ranked from low to high on the basis of VOD values and were pooled into bins of 250 grid cells. The mean of the corresponding AGC distribution in the reference map was calculated for each L-VOD bin, obtaining an AGC curve as a function of L-VOD[15]. The curve was fitted using the four-parameter function[23]:

$$\mathrm{AGC} = a \times \frac{\arctan(b \times (\mathrm{VOD} - c)) - \arctan(-b \times c)}{\arctan(b \times (\mathrm{Inf} - c)) - \arctan(-b \times c))} + d \quad (1)$$

where a, b, c and d are four best-fit parameters, Inf was set to 10^{10} and VOD is the yearly L-VOD data. The yearly L-VOD data calculated for 2011 (Supplementary Fig. 7f) was used in equation (1), as described by Rodriguez-Fernandez et al.[27], because 2011 was the first complete year after the SMOS commissioning phase.

We converted the yearly L-VOD map into maps of yearly AGC density (MgC ha^{-1}) for 2010–2017 using equation (1). Regional AGC stocks were obtained by multiplying the AGC density by the area of the corresponding L-VOD pixels.

AGC benchmark maps contain uncertainties and bias, and none can be considered reliable, as outlined above. We used all the different maps to fit equation (1) for tropical America, tropical Africa and the entire tropical region, separately. Benchmark maps in tropical Asia were not used in this calibration process due to the limited number of SMOS observations in the region. Ten calibrations of equation (1) were thereby obtained (Supplementary Table 1). We used all ten calibrations to create ten maps of AGC stocks. We used the median of these ten maps to calculate yearly tropical AGC maps during 2010–2017. The minima and maxima were also reported, because they provide estimates for the uncertainty of retrieved AGC estimates used in this study that relate to systematic errors in the reference biomass maps. A description of the computation of the uncertainties associated with the AGC estimates is given in the following section (a detailed description is provided in Supplementary Text 5).

Uncertainties associated with the AGC product. It is difficult to use independent datasets to validate the L-VOD-derived AGC estimates, as most reference biomass datasets are based on the same ICESat/GLAS LiDAR (Geoscience Laser Altimeter System instrument aboard the NASA Ice, Cloud and land Elevation satellite) dataset for areas of relatively high vegetation biomass.

We used a bootstrap and cross-validation approach to evaluate the 'internal' uncertainties (corresponding to sampling and calibration errors) associated with the L-VOD-derived AGC estimates. To account for 'external' uncertainties (uncertainties associated with the reference biomass maps) we used a very conservative approach in which the AGC estimates were derived as the median values of ten L-VOD derived AGC estimates. The ten estimates were computed from four reference biomass datasets (Baccini, Saatchi, Avitabile and Bouvet) calibrated against L-VOD over three different areas (the whole tropics, tropical Africa and tropical America). We used this subset of the Saatchi, Baccini and Avitabile datasets calibrated over three different areas and applied over the whole tropics in an attempt to account, in a realistic way, for the uncertainties associated with the parameters in equation (1). Then, the range (or spread) in the ten L-VOD derived AGC estimates was used as an indicator of the 'external' uncertainties associated with the AGC estimates. In a final step, we combined both external and internal uncertainties to obtain a more realistic estimate of the uncertainties associated with our calculation of AGC and AGC changes. A summary of the main conclusions of the analysis (Supplementary Text 5) is given below.

Based on a bootstrap cross-validation method, we found that internal errors (due to errors associated with sampling strategies and calibration errors) are almost negligible compared with external errors (due to uncertainties associated with the reference maps, and estimated here using a set of ten calibration functions). There is an order of magnitude between uncertainties arising from internal and external errors.

Considering combined internal and external errors, the relative uncertainties associated with the AGC stocks and changes in the AGC stocks over the tropics are on the order of 20–30%. Similar orders of magnitude were found at continental scales. We consider that this relative value is realistic, as it is based on a cross-validation approach considering sampling errors and a large set of ten different calibration functions.

As internal errors are almost an order of magnitude lower than external errors, and to simplify the computations of uncertainties, only external errors are considered in this study to compute uncertainties associated with the AGC stocks and AGC changes herein.

Additional uncertainties in the AGC product. The coarse spatial resolution of the AGC product failed to separate pixel-scale carbon gains and losses due to deforestation, regeneration, livestock pressure, conservation, fires and other events[15]. Moreover, the period of analysis covering two extreme climatic events (the 2011 La Niña and the 2010 and 2015–2016 El Niños) corresponding to strong carbon sinks and losses, increased the uncertainty in the trend analysis of the carbon changes in Fig. 2b. The main results of this study, however, do not rely on trend analysis but on spatial and temporal changes in carbon stocks. Open water bodies can affect the retrievals of L-VOD and soil moisture data[29,66], although SMOS-IC pixels in which the sum of the water fractions is greater than 10% have been filtered out using quality control flags provided by the SMOS-IC products[27].

Vegetation and climatic products. The types of vegetation cover in the present study included forest, shrubland, savannah, grassland, cropland and a mosaic of cropland and natural vegetation, which were identified using a 25 km International Geosphere–Biosphere Programme (IGBP) land-cover classification map[67] (Supplementary Fig. 6). The 25 km IGBP map was produced by aggregating the 500 m MODIS IGBP product into a 25 km resolution by dominant class within each SMOS L-VOD grid-resolution cell (Supplementary Text 1). Tropical semiarid biomes include shrubland, woodland and savannah regions based on the 25 km IGBP map[39].

We used the 'yearloss' forest area loss map[31] to calculate forest-loss rates. Forest loss was defined as a stand-replacement disturbance, or a change from a forest to a non-forest state[31,68]. Each 30 m pixel in the yearloss Landsat data was labelled with a loss year representing the loss of forest (defined as tree higher than 5 m) cover detected primarily during 2000–2017. Here, forest percentage loss rates during the study period 2010–2017 were calculated at the resolution of SMOS as the proportion of the summed areas of forest loss (detected by the yearloss map) within each SMOS-grid cell (~25 km) during 2010–2017.

The data used to compute trends in the annual average MODIS leaf-area index (LAI) (2010–2017) at a spatial resolution of 0.05° are provided by Chen et al.[32], who used the Mann–Kendall test to calculate the LAI trends on the basis of the MODIS LAI product (MOD15A2H and MYD15A2H). Greening and browning are defined as statistically significant increases and decreases, respectively, in the annual average green leaf area for a given pixel over 2010–2017[32].

The MOD100 annual forest area product used in this study (spatial resolution of 500 m) was produced from information on canopy phenology from the analyses of EVI and a land surface-water index derived from the MOD09A1 product[69]. The MOD100 product is a recent product using all the observations in a year (dense time series) from MOD09A1, and has shown excellent performance when compared against the official Brazilian deforestation dataset (PRODES) and Global Forest Watch[70].

We used the annual mean global CO_2 growth-rate data for 2010–2017, based on globally averaged marine surface data, compiled and published by the National Oceanic and Atmospheric Administration Earth System Research Laboratory in Colorado.

Several vegetation and climate variables (Supplementary Table 4) were used to further investigate the response of AGC to climate events. These variables include: (1) the multivariate El Niño/Southern Oscillation index (MEI)[71]; (2) EVI from the MODIS vegetation index product (MOD13C2 Climate Modeling Grid)[72], (3) land surface temperature from skin temperature data produced by European Centre for Medium-Range Weather Forecasts atmospheric reanalysis ERA-Interim[73], (4) precipitation from datasets of the Tropical Rainfall Measuring Mission (TRMM 3B43 v.7)[74] and (5) terrestrial water storage (TWS) measured by the twin satellites of the gravity recovery and climate experiment (GRACE) providing the total relative water storage including groundwater, soil moisture, surface water, snow and water stored in the biosphere[75,76]. Monthly TWS was calculated as a simple arithmetic mean of three datasets, the monthly 1° GRACE TWS products released

by the Jet Propulsion Laboratory; the Centre for Space Research, University of Texas; and the German Research Centre for Geosciences; and was then aggregated to yearly TWS[77].

EVI, precipitation and land surface temperature were aggregated to an annual composite at 25 km spatial resolution by averaging or bilinear interpolation from their original resolution to match the L-VOD grid.

Statistical metrics. We calculated two goodness-of-fit metrics between pairs of reference benchmark map and AGC map: r^2 and the r.m.s. error (MgC ha^{-1}). Trend estimates were calculated using linear regression slope. Linear correlation coefficients (Pearson's r) were calculated to quantify the concurrent association between time series. The levels of statistical significance (P values) were estimated throughout this analysis, and the correlation coefficients r were considered to be statistically significant if the P values were less than 0.05.

Reporting Summary. Further information on research design is available in the Nature Research Reporting Summary linked to this article.

Data availability

The IGBP land-cover classification map, EVI, forest area loss map, GRACE data for terrestrial groundwater storage, precipitation data, skin temperature product, global CO_2 growth-rate data, MEI and the Baccini and Avitabile biomass maps are publicly available. The SMOS-IC soil moisture dataset is available via Centre Aval de Traitement des Données SMOS at http://www.catds.fr/Products/Available-products-from-CEC-SM/SMOS-IC. SMOS-IC L-VOD and AGC products, the Saatchi, Bouvet and Mermoz biomass maps are available from J.-P.W., S.S.S. (sasan.s.saatchi@jpl.nasa.gov), A. Bouvet (alexandre.bouvet@cesbio.cnes.fr) and S. Mermoz (stephane.mermoz@cesbio.cnes.fr) both at CESBIO, Toulouse, France), respectively, on request.

Received: 18 January 2019; Accepted: 19 June 2019;
Published online: 29 July 2019

References

1. Mitchard, E. T. A. The tropical forest carbon cycle and climate change. *Nature* **559**, 527–534 (2018).
2. Hansen, M. C., Potapov, P. & Tyukavina, A. Comment on "Tropical forests are a net carbon source based on aboveground measurements of gain and loss". *Science* **363**, eaar3629 (2019).
3. Saatchi, S. S. et al. Benchmark map of forest carbon stocks in tropical regions across three continents. *Proc. Natl Acad. Sci. USA* **108**, 9899–9904 (2011).
4. Gaubert, B. et al. Global atmospheric CO_2 inverse models converging on neutral tropical land exchange, but disagreeing on fossil fuel and atmospheric growth rate. *Biogeosciences* **16**, 117–134 (2019).
5. Baccini, A. et al. Estimated carbon dioxide emissions from tropical deforestation improved by carbon-density maps. *Nat. Clim. Change* **2**, 182 (2012).
6. Harris, N. L. et al. Baseline map of carbon emissions from deforestation in tropical regions. *Science* **336**, 1573–1576 (2012).
7. Achard, F. et al. Determination of tropical deforestation rates and related carbon losses from 1990 to 2010. *Glob. Change Biol.* **20**, 2540–2554 (2014).
8. Chazdon, R. L. et al. Carbon sequestration potential of second-growth forest regeneration in the Latin American tropics. *Sci. Adv.* **2**, e1501639 (2016).
9. Yang, Y. et al. Post-drought decline of the Amazon carbon sink. *Nat. Commun.* **9**, 3172 (2018).
10. Brienen, R. J. et al. Long-term decline of the Amazon carbon sink. *Nature* **519**, 344 (2015).
11. Pan, Y. et al. A large and persistent carbon sink in the world's forests. *Science* **333**, 988–993 (2011). 1201609.
12. Malhi, Y. The productivity, metabolism and carbon cycle of tropical forest vegetation. *J. Ecol.* **100**, 65–75 (2012).
13. Liu, J. et al. Contrasting carbon cycle responses of the tropical continents to the 2015–2016 El Niño. *Science* **358**, eaam5690 (2017).
14. Yue, C. et al. Vegetation greenness and land carbon-flux anomalies associated with climate variations: a focus on the year 2015. *Atmos. Chem. Phys.* **17**, 13903–13919 (2017).
15. Brandt, M. et al. Satellite passive microwaves reveal recent climate-induced carbon losses in African drylands. *Nat. Ecol. Evol.* **2**, 827–835 (2018).
16. Bastos, A. et al. Impact of the 2015/2016 El Niño on the terrestrial carbon cycle constrained by bottom-up and top-down approaches. *Phil. Trans. R. Soc. B* **373**, 20170304 (2018).
17. Baccini, A. et al. Tropical forests are a net carbon source based on aboveground measurements of gain and loss. *Science* **358**, 230–234 (2017).
18. Avitabile, V. et al. An integrated pan-tropical biomass map using multiple reference datasets. *Glob. Change Biol.* **22**, 1406–1420 (2016).
19. Bouvet, A. et al. An above-ground biomass map of African savannahs and woodlands at 25 m resolution derived from ALOS PALSAR. *Remote Sens. Environ.* **206**, 156–173 (2018).
20. Konings, A. G. & Gentine, P. Global variations in ecosystem-scale isohydricity. *Glob. Change Biol.* **23**, 891–905 (2017).
21. Konings, A., Williams, A. & Gentine, P. Sensitivity of grassland productivity to aridity controlled by stomatal and xylem regulation. *Nat. Geosci.* **10**, 284–288 (2017).
22. Wigneron, J.-P., Kerr, Y., Chanzy, A. & Jin, Y.-Q. Inversion of surface parameters from passive microwave measurements over a soybean field. *Remote Sens. Environ.* **46**, 61–72 (1993).
23. Liu, Y. Y. et al. Recent reversal in loss of global terrestrial biomass. *Nat. Clim. Change* **5**, 470–474 (2015).
24. Liu, Y. Y., van Dijk, A. I., McCabe, M. F., Evans, J. P. & de Jeu, R. A. Global vegetation biomass change (1988–2008) and attribution to environmental and human drivers. *Glob. Ecol. Biogeogr.* **22**, 692–705 (2013).
25. Wigneron, J.-P. et al. Modelling the passive microwave signature from land surfaces: A review of recent results and application to the L-band SMOS & SMAP soil moisture retrieval algorithms. *Remote Sens. Environ.* **192**, 238–262 (2017).
26. Fernandez-Moran, R. et al. SMOS-IC: An alternative SMOS soil moisture and vegetation optical depth product. *Remote Sens.* **9**, 457 (2017).
27. Rodríguez-Fernández, N. J. et al. An evaluation of SMOS L-band vegetation optical depth (L-VOD) data sets: high sensitivity of L-VOD to above-ground biomass in Africa. *Biogeosciences* **15**, 4627–4645 (2018).
28. Tian, F. et al. Coupling of ecosystem-scale plant water storage and leaf phenology observed by satellite. *Nat. Ecol. Evol.* **2**, 1428–1435 (2018).
29. Liu, Y. Y., de Jeu, R. A., McGabe, M. F., Evans, J. P. & van Dijk, A. I. Global long-term passive microwave satellite-based retrievals of vegetation optical depth. *Geophys. Res. Lett.* **38**, L18402 (2011).
30. Poulter, B. et al. Contribution of semi-arid ecosystems to interannual variability of the global carbon cycle. *Nature* **509**, 600–603 (2014).
31. Hansen, M. C. et al. High-resolution global maps of 21st-century forest cover change. *Science* **342**, 850–853 (2013).
32. Chen, C. et al. China and India lead in greening of the world through land-use management. *Nat. Sustain.* **2**, 122–129 (2019).
33. Humphrey, V. et al. Sensitivity of atmospheric CO_2 growth rate to observed changes in terrestrial water storage. *Nature* **560**, 628–631 (2018).
34. Jung, M. et al. Compensatory water effects link yearly global land CO_2 sink changes to temperature. *Nature* **541**, 516–520 (2017).
35. Masarie, K. A. & Tans, P. P. Extension and integration of atmospheric carbon dioxide data into a globally consistent measurement record. *J. Geophys. Res.* **100**, 11593–11610 (1995).
36. Wang, J., Zeng, N. & Wang, M. Interannual variability of the atmospheric CO_2 growth rate: roles of precipitation and temperature. *Biogeosciences* **13**, 2339–2352 (2016).
37. Zeng, N., Mariotti, A. & Wetzel, P. Terrestrial mechanisms of interannual CO_2 variability. *Glob. Biogeochem. Cycles* **19**, GB1016 (2005).
38. Anderegg, W. R. et al. Tropical nighttime warming as a dominant driver of variability in the terrestrial carbon sink. *Proc. Natl Acad. Sci. USA* **112**, 15591–15596 (2015).
39. Ahlström, A. et al. The dominant role of semi-arid ecosystems in the trend and variability of the land CO_2 sink. *Science* **348**, 895–899 (2015).
40. Fernández-Martínez, M. et al. Global trends in carbon sinks and their relationships with CO_2 and temperature. *Nat. Clim. Change* **9**, 73–79 (2019).
41. Lohberger, S., Stängel, M., Atwood, E. C. & Siegert, F. Spatial evaluation of Indonesia's 2015 fire-affected area and estimated carbon emissions using Sentinel-1. *Glob. Change Biol.* **24**, 644–654 (2018).
42. Huijnen, V. et al. Fire carbon emissions over maritime Southeast Asia in 2015 largest since 1997. *Sci. Rep.* **6**, 26886 (2016).
43. Yin, Y. et al. Variability of fire carbon emissions in equatorial Asia and its nonlinear sensitivity to El Niño. *Geophys. Res. Lett.* **43**, 10472–10479 (2016).
44. Tyukavina, A. et al. Aboveground carbon loss in natural and managed tropical forests from 2000 to 2012. *Environ. Res. Lett.* **10**, 074002 (2015).
45. Zarin, D. J. et al. Can carbon emissions from tropical deforestation drop by 50% in 5 years? *Glob. Change Biol.* **22**, 1336–1347 (2016).
46. Ryan, C. M., Berry, N. J. & Joshi, N. Quantifying the causes of deforestation and degradation and creating transparent REDD+ baselines: a method and case study from central Mozambique. *Appl. Geogr.* **53**, 45–54 (2014).
47. Ponce-Campos, G. E. et al. Ecosystem resilience despite large-scale altered hydroclimatic conditions. *Nature* **494**, 349–352 (2013).
48. Poorter, L. et al. Biomass resilience of neotropical secondary forests. *Nature* **530**, 211–214 (2016).
49. Lewis, S. L. et al. Increasing carbon storage in intact African tropical forests. *Nature* **457**, 1003–1006 (2009).
50. Phillips, O. L. et al. Changes in the carbon balance of tropical forests: evidence from long-term plots. *Science* **282**, 439–442 (1998).
51. Gloor, M. et al. Does the disturbance hypothesis explain the biomass increase in basin-wide Amazon forest plot data? *Glob. Change Biol.* **15**, 2418–2430 (2009).
52. Zhu, Z. et al. Greening of the Earth and its drivers. *Nat. Clim.* **6**, 791–795 (2016).

53. Brandt, M. et al. Changes in rainfall distribution promote woody foliage production in the Sahel. *Commun. Biol.* **2**, 133 (2019).
54. Schimel, D., Stephens, B. B. & Fisher, J. B. Effect of increasing CO_2 on the terrestrial carbon cycle. *Proc. Natl Acad. Sci. USA* **112**, 436–441 (2015).
55. Rutishauser, E. et al. Rapid tree carbon stock recovery in managed Amazonian forests. *Curr. Biol.* **25**, R787–R788 (2015).
56. Brandt, M. et al. Human population growth offsets climate-driven increase in woody vegetation in sub-Saharan Africa. *Nat. Ecol. Evol.* **1**, 0081 (2017).
57. Jackson, T. & Schmugge, T. Vegetation effects on the microwave emission of soils. *Remote Sens. Environ.* **36**, 203–212 (1991).
58. Wigneron, J.-P., Waldteufel, P., Chanzy, A., Calvet, J.-C. & Kerr, Y. Two-dimensional microwave interferometer retrieval capabilities over land surfaces (SMOS mission). *Remote Sens. Environ.* **73**, 270–282 (2000).
59. Al-Yaari, A. et al. Assessment and inter-comparison of recently developed/reprocessed microwave satellite soil moisture products using ISMN ground-based measurements. *Remote Sens. Environ.* **224**, 289–303 (2019).
60. Carreiras, J. M. et al. Coverage of high biomass forests by the ESA BIOMASS mission under defense restrictions. *Remote Sens. Environ.* **196**, 154–162 (2017).
61. Mermoz, S., Le Toan, T., Villard, L., Réjou-Méchain, M. & Seifert-Granzin, J. Biomass assessment in the Cameroon savanna using ALOS PALSAR data. *Remote Sens. Environ.* **155**, 109–119 (2014).
62. Wigneron, J.-P. et al. L-band microwave emission of the biosphere (L-MEB) model: description and calibration against experimental data sets over crop fields. *Remote Sens. Environ.* **107**, 639–655 (2007).
63. Kerr, Y. H. et al. The SMOS soil moisture retrieval algorithm. *IEEE Trans. Geosci. Remote Sens.* **50**, 1384–1403 (2012).
64. Oliva, R. et al. SMOS radio frequency interference scenario: status and actions taken to improve the RFI environment in the 1400–1427-MHz passive band. *IEEE Trans. Geosci. Remote Sens.* **50**, 1427–1439 (2012).
65. Kerr, Y. H. et al. Overview of SMOS performance in terms of global soil moisture monitoring after six years in operation. *Remote Sens. Environ.* **180**, 40–63 (2016).
66. Fan, L. et al. Evaluation of microwave remote sensing for monitoring live fuel moisture content in the Mediterranean region. *Remote Sens. Environ.* **205**, 210–223 (2018).
67. Broxton, P. D., Zeng, X., Sulla-Menashe, D. & Troch, P. A. A global land cover climatology using MODIS data. *J. Appl. Meteorol. Climatol.* **53**, 1593–1605 (2014).
68. Hansen, M. C., Stehman, S. V. & Potapov, P. V. Quantification of global gross forest cover loss. *Proc. Natl Acad. Sci. USA* **107**, 8650–8655 (2010).
69. Qin, Y. et al. Annual dynamics of forest areas in South America during 2007–2010 at 50-m spatial resolution. *Remote Sens. Environ.* **201**, 73–87 (2017).
70. Qin, Y. et al. Improved estimates of forest cover and loss in the Brazilian Amazon in 2000–2017. *Nat. Sustain.* (in the press).
71. Wolter, K. & Timlin, M. S. El Niño/Southern oscillation behaviour since 1871 as diagnosed in an extended multivariate ENSO index (MEI.ext). *Int. J. Climatol.* **31**, 1074–1087 (2011).
72. Huete, A. R., Justice, C. O. & Van Leeuwen, W. *MODIS Vegetation Index (MOD13). Algorithm Theoretical Basis Document* (NASA, 1999); https://modis.gsfc.nasa.gov/data/atbd/atbd_mod13.pdf
73. Dee, D. P. et al. The ERA-Interim reanalysis: configuration and performance of the data assimilation system. *Q. J. R. Meteorol. Soc.* **137**, 553–597 (2011).
74. Huffman, G. J. et al. The TRMM multisatellite precipitation analysis (TMPA): quasi-global, multiyear, combined-sensor precipitation estimates at fine scales. *J. Hydrometeorol.* **8**, 38–55 (2007).
75. Wahr, J., Molenaar, M. & Bryan, F. Time variability of the Earth's gravity field: hydrological and oceanic effects and their possible detection using GRACE. *J. Geophys. Res.* **103**, 30205–30229 (1998).
76. Swenson, S., Chambers, D. & Wahr, J. Estimating geocenter variations from a combination of GRACE and ocean model output. *J. Geophys. Res.* **113**, B08410 (2008).
77. Liu, Y. Y. et al. Enhanced canopy growth precedes senescence in 2005 and 2010 Amazonian droughts. *Remote Sens. Environ.* **211**, 26–37 (2018).

Acknowledgements

This work was jointly supported by the TOSCA (Terre Océan Surfaces Continentales et Atmosphère) CNES (Centre National d'Etudes Spatiales) programme, the European Space Agency Support to Science Element programme and SMOS Expert Support Laboratory contract, and the European Research Council Synergy grant ERC-2013-SyG-610028 IMBALANCE-P. P.C. acknowledges additional support from the ANR ICONV CLAND grant. J.C. has benefited from 'Investissement d'Avenir' grants managed by Agence Nationale de la Recherche (CEBA: ANR-10-LABX- 25-01; TULIP: ANR-10-LABX-0041; ANAEE-France: ANR-11-INBS-0001). M.B. was funded by an AXA postdoctoral fellowship. F.T. is supported by a Marie Skłodowska-Curie grant (project number 746347). R.F. acknowledges funding from the Danish Council for Independent Research (DFF) grant no. DFF–6111-00258. K.H. acknowledges support by the Belgian Science Policy Office-sponsored COBECORE project (contract BR/175/A3/COBECORE). L.F. acknowledges additional support from the National Natural Science Foundation of China (grant no. 41801247) and Natural Science Foundation of Jiangsu Province (grant no. BK20180806). Y.Q. and X.X. are supported in part by NASA Land Use and Land Cover Change programme (NNX14AD78G) and NASA Geostationary Carbon Cycle Observatory (GeoCarb) Mission (GeoCarb contract no. 80LARC17C0001).

Author contributions

J.-P.W., L.F. and P.C. conceived and designed the study. L.F. carried out all calculations with support from J.-P.W. and P.C. L.F. prepared the SMOS-IC data; S.S.S. prepared the Saatchi biomass map; Y.Q. and X.X. prepared annual forest area maps; C.C. and R.B.M. prepared the MODIS LAI dataset. J.-P.W., L.F. and P.C. conducted the analysis with support from J.C., M.B., R.F., S.S.S., J.P. and A.B. The manuscript was drafted by L.F., J.-P.W., P.C., J.C., R.F., M.B., J.P., K.H. with contributions by all co-authors.

Additional information

Supplementary information is available for this paper at https://doi.org/10.1038/s41477-019-0478-9.

Reprints and permissions information is available at www.nature.com/reprints.

Correspondence and requests for materials should be addressed to J.-P.W. or P.C.

Peer review information: *Nature Plants* thanks Edward Mitchard, Kolby Smith and the other, anonymous, reviewers for their contribution to the peer review of this work.

Publisher's note: Springer Nature remains neutral with regard to jurisdictional claims in published maps and institutional affiliations.

© The Author(s), under exclusive licence to Springer Nature Limited 2019

nature research

Corresponding author(s): Jean-Pierre WIGNERON

Last updated by author(s): Jun 18, 2019

Reporting Summary

Nature Research wishes to improve the reproducibility of the work that we publish. This form provides structure for consistency and transparency in reporting. For further information on Nature Research policies, see Authors & Referees and the Editorial Policy Checklist.

Statistics

For all statistical analyses, confirm that the following items are present in the figure legend, table legend, main text, or Methods section.

n/a	Confirmed	
☐	☒	The exact sample size (*n*) for each experimental group/condition, given as a discrete number and unit of measurement
☐	☒	A statement on whether measurements were taken from distinct samples or whether the same sample was measured repeatedly
☐	☒	The statistical test(s) used AND whether they are one- or two-sided *Only common tests should be described solely by name; describe more complex techniques in the Methods section.*
☐	☒	A description of all covariates tested
☐	☒	A description of any assumptions or corrections, such as tests of normality and adjustment for multiple comparisons
☐	☒	A full description of the statistical parameters including central tendency (e.g. means) or other basic estimates (e.g. regression coefficient) AND variation (e.g. standard deviation) or associated estimates of uncertainty (e.g. confidence intervals)
☐	☐	For null hypothesis testing, the test statistic (e.g. *F*, *t*, *r*) with confidence intervals, effect sizes, degrees of freedom and *P* value noted *Give P values as exact values whenever suitable.*
☐	☐	For Bayesian analysis, information on the choice of priors and Markov chain Monte Carlo settings
☐	☐	For hierarchical and complex designs, identification of the appropriate level for tests and full reporting of outcomes
☐	☒	Estimates of effect sizes (e.g. Cohen's *d*, Pearson's *r*), indicating how they were calculated

Our web collection on statistics for biologists contains articles on many of the points above.

Software and code

Policy information about availability of computer code

Data collection	all data were downloaded from institutional sites; all these data are either open access or available upon request; The SMOS-IC L-VOD data set is available upon request to the corresponding author; a description of data availability is given in the text
Data analysis	Matlab, and open softwares as R and Python

For manuscripts utilizing custom algorithms or software that are central to the research but not yet described in published literature, software must be made available to editors/reviewers. We strongly encourage code deposition in a community repository (e.g. GitHub). See the Nature Research guidelines for submitting code & software for further information.

Data

Policy information about availability of data

All manuscripts must include a data availability statement. This statement should provide the following information, where applicable:

- Accession codes, unique identifiers, or web links for publicly available datasets
- A list of figures that have associated raw data
- A description of any restrictions on data availability

IGBP land-cover classification map, EVI, Forest area loss map, GRACE data for terrestrial groundwater storage, precipitation data, skin temperature product, global CO2 growth rate data, Multivariate ENSO Index (MEI), the Baccini and Avitabile biomass maps are publicly available. SMOS-IC soil moisture dataset are available via CATDS at http://www.catds.fr/Products/Available-products-from-CEC-SM/SMOS-IC. SMOS-IC L-VOD and AGC products, the Saatchi and Bouvet-Mermoz biomass maps are available from the corresponding authors upon request.

Field-specific reporting

Please select the one below that is the best fit for your research. If you are not sure, read the appropriate sections before making your selection.

☐ Life sciences ☐ Behavioural & social sciences ☐ Ecological, evolutionary & environmental sciences

For a reference copy of the document with all sections, see nature.com/documents/nr-reporting-summary-flat.pdf

Life sciences study design

All studies must disclose on these points even when the disclosure is negative.

Sample size	*Describe how sample size was determined, detailing any statistical methods used to predetermine sample size OR if no sample-size calculation was performed, describe how sample sizes were chosen and provide a rationale for why these sample sizes are sufficient.*
Data exclusions	*Describe any data exclusions. If no data were excluded from the analyses, state so OR if data were excluded, describe the exclusions and the rationale behind them, indicating whether exclusion criteria were pre-established.*
Replication	*Describe the measures taken to verify the reproducibility of the experimental findings. If all attempts at replication were successful, confirm this OR if there are any findings that were not replicated or cannot be reproduced, note this and describe why.*
Randomization	*Describe how samples/organisms/participants were allocated into experimental groups. If allocation was not random, describe how covariates were controlled OR if this is not relevant to your study, explain why.*
Blinding	*Describe whether the investigators were blinded to group allocation during data collection and/or analysis. If blinding was not possible, describe why OR explain why blinding was not relevant to your study.*

Behavioural & social sciences study design

All studies must disclose on these points even when the disclosure is negative.

Study description	*Briefly describe the study type including whether data are quantitative, qualitative, or mixed-methods (e.g. qualitative cross-sectional, quantitative experimental, mixed-methods case study).*
Research sample	*State the research sample (e.g. Harvard university undergraduates, villagers in rural India) and provide relevant demographic information (e.g. age, sex) and indicate whether the sample is representative. Provide a rationale for the study sample chosen. For studies involving existing datasets, please describe the dataset and source.*
Sampling strategy	*Describe the sampling procedure (e.g. random, snowball, stratified, convenience). Describe the statistical methods that were used to predetermine sample size OR if no sample-size calculation was performed, describe how sample sizes were chosen and provide a rationale for why these sample sizes are sufficient. For qualitative data, please indicate whether data saturation was considered, and what criteria were used to decide that no further sampling was needed.*
Data collection	*Provide details about the data collection procedure, including the instruments or devices used to record the data (e.g. pen and paper, computer, eye tracker, video or audio equipment) whether anyone was present besides the participant(s) and the researcher, and whether the researcher was blind to experimental condition and/or the study hypothesis during data collection.*
Timing	*Indicate the start and stop dates of data collection. If there is a gap between collection periods, state the dates for each sample cohort.*
Data exclusions	*If no data were excluded from the analyses, state so OR if data were excluded, provide the exact number of exclusions and the rationale behind them, indicating whether exclusion criteria were pre-established.*
Non-participation	*State how many participants dropped out/declined participation and the reason(s) given OR provide response rate OR state that no participants dropped out/declined participation.*
Randomization	*If participants were not allocated into experimental groups, state so OR describe how participants were allocated to groups, and if allocation was not random, describe how covariates were controlled.*

Ecological, evolutionary & environmental sciences study design

All studies must disclose on these points even when the disclosure is negative.

Study description	*Briefly describe the study. For quantitative data include treatment factors and interactions, design structure (e.g. factorial, nested, hierarchical), nature and number of experimental units and replicates.*
Research sample	*Describe the research sample (e.g. a group of tagged Passer domesticus, all Stenocereus thurberi within Organ Pipe Cactus National*

Research sample	*Monument), and provide a rationale for the sample choice. When relevant, describe the organism taxa, source, sex, age range and any manipulations. State what population the sample is meant to represent when applicable. For studies involving existing datasets, describe the data and its source.*
Sampling strategy	*Note the sampling procedure. Describe the statistical methods that were used to predetermine sample size OR if no sample-size calculation was performed, describe how sample sizes were chosen and provide a rationale for why these sample sizes are sufficient.*
Data collection	*Describe the data collection procedure, including who recorded the data and how.*
Timing and spatial scale	*Indicate the start and stop dates of data collection, noting the frequency and periodicity of sampling and providing a rationale for these choices. If there is a gap between collection periods, state the dates for each sample cohort. Specify the spatial scale from which the data are taken*
Data exclusions	*If no data were excluded from the analyses, state so OR if data were excluded, describe the exclusions and the rationale behind them, indicating whether exclusion criteria were pre-established.*
Reproducibility	*Describe the measures taken to verify the reproducibility of experimental findings. For each experiment, note whether any attempts to repeat the experiment failed OR state that all attempts to repeat the experiment were successful.*
Randomization	*Describe how samples/organisms/participants were allocated into groups. If allocation was not random, describe how covariates were controlled. If this is not relevant to your study, explain why.*
Blinding	*Describe the extent of blinding used during data acquisition and analysis. If blinding was not possible, describe why OR explain why blinding was not relevant to your study.*

Did the study involve field work? ☐ Yes ☐ No

Field work, collection and transport

Field conditions	*Describe the study conditions for field work, providing relevant parameters (e.g. temperature, rainfall).*
Location	*State the location of the sampling or experiment, providing relevant parameters (e.g. latitude and longitude, elevation, water depth).*
Access and import/export	*Describe the efforts you have made to access habitats and to collect and import/export your samples in a responsible manner and in compliance with local, national and international laws, noting any permits that were obtained (give the name of the issuing authority, the date of issue, and any identifying information).*
Disturbance	*Describe any disturbance caused by the study and how it was minimized.*

Reporting for specific materials, systems and methods

We require information from authors about some types of materials, experimental systems and methods used in many studies. Here, indicate whether each material, system or method listed is relevant to your study. If you are not sure if a list item applies to your research, read the appropriate section before selecting a response.

Materials & experimental systems

n/a	Involved in the study
☐	☐ Antibodies
☐	☐ Eukaryotic cell lines
☐	☐ Palaeontology
☐	☐ Animals and other organisms
☐	☐ Human research participants
☐	☐ Clinical data

Methods

n/a	Involved in the study
☐	☐ ChIP-seq
☐	☐ Flow cytometry
☐	☐ MRI-based neuroimaging

Antibodies

Antibodies used	*Describe all antibodies used in the study; as applicable, provide supplier name, catalog number, clone name, and lot number.*
Validation	*Describe the validation of each primary antibody for the species and application, noting any validation statements on the manufacturer's website, relevant citations, antibody profiles in online databases, or data provided in the manuscript.*

Eukaryotic cell lines

Policy information about cell lines

Cell line source(s)	*State the source of each cell line used.*
Authentication	*Describe the authentication procedures for each cell line used OR declare that none of the cell lines used were authenticated.*
Mycoplasma contamination	*Confirm that all cell lines tested negative for mycoplasma contamination OR describe the results of the testing for mycoplasma contamination OR declare that the cell lines were not tested for mycoplasma contamination.*
Commonly misidentified lines (See ICLAC register)	*Name any commonly misidentified cell lines used in the study and provide a rationale for their use.*

Palaeontology

Specimen provenance	*Provide provenance information for specimens and describe permits that were obtained for the work (including the name of the issuing authority, the date of issue, and any identifying information).*
Specimen deposition	*Indicate where the specimens have been deposited to permit free access by other researchers.*
Dating methods	*If new dates are provided, describe how they were obtained (e.g. collection, storage, sample pretreatment and measurement), where they were obtained (i.e. lab name), the calibration program and the protocol for quality assurance OR state that no new dates are provided.*

☐ Tick this box to confirm that the raw and calibrated dates are available in the paper or in Supplementary Information.

Animals and other organisms

Policy information about studies involving animals; ARRIVE guidelines recommended for reporting animal research

Laboratory animals	*For laboratory animals, report species, strain, sex and age OR state that the study did not involve laboratory animals.*
Wild animals	*Provide details on animals observed in or captured in the field; report species, sex and age where possible. Describe how animals were caught and transported and what happened to captive animals after the study (if killed, explain why and describe method; if released, say where and when) OR state that the study did not involve wild animals.*
Field-collected samples	*For laboratory work with field-collected samples, describe all relevant parameters such as housing, maintenance, temperature, photoperiod and end-of-experiment protocol OR state that the study did not involve samples collected from the field.*
Ethics oversight	*Identify the organization(s) that approved or provided guidance on the study protocol, OR state that no ethical approval or guidance was required and explain why not.*

Note that full information on the approval of the study protocol must also be provided in the manuscript.

Human research participants

Policy information about studies involving human research participants

Population characteristics	*Describe the covariate-relevant population characteristics of the human research participants (e.g. age, gender, genotypic information, past and current diagnosis and treatment categories). If you filled out the behavioural & social sciences study design questions and have nothing to add here, write "See above."*
Recruitment	*Describe how participants were recruited. Outline any potential self-selection bias or other biases that may be present and how these are likely to impact results.*
Ethics oversight	*Identify the organization(s) that approved the study protocol.*

Note that full information on the approval of the study protocol must also be provided in the manuscript.

Clinical data

Policy information about clinical studies

All manuscripts should comply with the ICMJE guidelines for publication of clinical research and a completed CONSORT checklist must be included with all submissions.

Clinical trial registration	*Provide the trial registration number from ClinicalTrials.gov or an equivalent agency.*
Study protocol	*Note where the full trial protocol can be accessed OR if not available, explain why.*
Data collection	*Describe the settings and locales of data collection, noting the time periods of recruitment and data collection.*

Outcomes — *Describe how you pre-defined primary and secondary outcome measures and how you assessed these measures.*

ChIP-seq

Data deposition

☐ Confirm that both raw and final processed data have been deposited in a public database such as GEO.

☐ Confirm that you have deposited or provided access to graph files (e.g. BED files) for the called peaks.

Data access links
May remain private before publication.
For "Initial submission" or "Revised version" documents, provide reviewer access links. For your "Final submission" document, provide a link to the deposited data.

Files in database submission — *Provide a list of all files available in the database submission.*

Genome browser session
(e.g. UCSC)
Provide a link to an anonymized genome browser session for "Initial submission" and "Revised version" documents only, to enable peer review. Write "no longer applicable" for "Final submission" documents.

Methodology

Replicates — *Describe the experimental replicates, specifying number, type and replicate agreement.*

Sequencing depth — *Describe the sequencing depth for each experiment, providing the total number of reads, uniquely mapped reads, length of reads and whether they were paired- or single-end.*

Antibodies — *Describe the antibodies used for the ChIP-seq experiments; as applicable, provide supplier name, catalog number, clone name, and lot number.*

Peak calling parameters — *Specify the command line program and parameters used for read mapping and peak calling, including the ChIP, control and index files used.*

Data quality — *Describe the methods used to ensure data quality in full detail, including how many peaks are at FDR 5% and above 5-fold enrichment.*

Software — *Describe the software used to collect and analyze the ChIP-seq data. For custom code that has been deposited into a community repository, provide accession details.*

Flow Cytometry

Plots

Confirm that:

☐ The axis labels state the marker and fluorochrome used (e.g. CD4-FITC).

☐ The axis scales are clearly visible. Include numbers along axes only for bottom left plot of group (a 'group' is an analysis of identical markers).

☐ All plots are contour plots with outliers or pseudocolor plots.

☐ A numerical value for number of cells or percentage (with statistics) is provided.

Methodology

Sample preparation — *Describe the sample preparation, detailing the biological source of the cells and any tissue processing steps used.*

Instrument — *Identify the instrument used for data collection, specifying make and model number.*

Software — *Describe the software used to collect and analyze the flow cytometry data. For custom code that has been deposited into a community repository, provide accession details.*

Cell population abundance — *Describe the abundance of the relevant cell populations within post-sort fractions, providing details on the purity of the samples and how it was determined.*

Gating strategy — *Describe the gating strategy used for all relevant experiments, specifying the preliminary FSC/SSC gates of the starting cell population, indicating where boundaries between "positive" and "negative" staining cell populations are defined.*

☐ Tick this box to confirm that a figure exemplifying the gating strategy is provided in the Supplementary Information.

Magnetic resonance imaging

Experimental design

Design type	*Indicate task or resting state; event-related or block design.*
Design specifications	*Specify the number of blocks, trials or experimental units per session and/or subject, and specify the length of each trial or block (if trials are blocked) and interval between trials.*
Behavioral performance measures	*State number and/or type of variables recorded (e.g. correct button press, response time) and what statistics were used to establish that the subjects were performing the task as expected (e.g. mean, range, and/or standard deviation across subjects).*

Acquisition

Imaging type(s)	*Specify: functional, structural, diffusion, perfusion.*
Field strength	*Specify in Tesla*
Sequence & imaging parameters	*Specify the pulse sequence type (gradient echo, spin echo, etc.), imaging type (EPI, spiral, etc.), field of view, matrix size, slice thickness, orientation and TE/TR/flip angle.*
Area of acquisition	*State whether a whole brain scan was used OR define the area of acquisition, describing how the region was determined.*

Diffusion MRI ☐ Used ☐ Not used

Preprocessing

Preprocessing software	*Provide detail on software version and revision number and on specific parameters (model/functions, brain extraction, segmentation, smoothing kernel size, etc.).*
Normalization	*If data were normalized/standardized, describe the approach(es): specify linear or non-linear and define image types used for transformation OR indicate that data were not normalized and explain rationale for lack of normalization.*
Normalization template	*Describe the template used for normalization/transformation, specifying subject space or group standardized space (e.g. original Talairach, MNI305, ICBM152) OR indicate that the data were not normalized.*
Noise and artifact removal	*Describe your procedure(s) for artifact and structured noise removal, specifying motion parameters, tissue signals and physiological signals (heart rate, respiration).*
Volume censoring	*Define your software and/or method and criteria for volume censoring, and state the extent of such censoring.*

Statistical modeling & inference

Model type and settings	*Specify type (mass univariate, multivariate, RSA, predictive, etc.) and describe essential details of the model at the first and second levels (e.g. fixed, random or mixed effects; drift or auto-correlation).*
Effect(s) tested	*Define precise effect in terms of the task or stimulus conditions instead of psychological concepts and indicate whether ANOVA or factorial designs were used.*

Specify type of analysis: ☐ Whole brain ☐ ROI-based ☐ Both

Statistic type for inference (See Eklund et al. 2016)	*Specify voxel-wise or cluster-wise and report all relevant parameters for cluster-wise methods.*
Correction	*Describe the type of correction and how it is obtained for multiple comparisons (e.g. FWE, FDR, permutation or Monte Carlo).*

Models & analysis

n/a	Involved in the study
☐	☐ Functional and/or effective connectivity
☐	☐ Graph analysis
☐	☐ Multivariate modeling or predictive analysis

Functional and/or effective connectivity	*Report the measures of dependence used and the model details (e.g. Pearson correlation, partial correlation, mutual information).*
Graph analysis	*Report the dependent variable and connectivity measure, specifying weighted graph or binarized graph, subject- or group-level, and the global and/or node summaries used (e.g. clustering coefficient, efficiency, etc.).*

Multivariate modeling and predictive analysis

Specify independent variables, features extraction and dimension reduction, model, training and evaluation metrics.